Electronic Supplementary Material (ESI) for Journal of Materials Chemistry C.

Supporting information for:

Colloidal Synthesis of Lead-free $Cs_2TiBr_{6-x}I_x$ Perovskite Nanocrystals

Shanti Maria Liga,[a] Gerasimos Konstantatos*[,a,b]

[a]ICFO, Institut de Ciencies Fotoniques, The Barcelona Institute of Science and Technology, 08860 Castelldefels, Barcelona, Spain;

[b]ICREA, Institució Catalana de Recerca i Estudis Avançats, 08010 Barcelona, Spain;

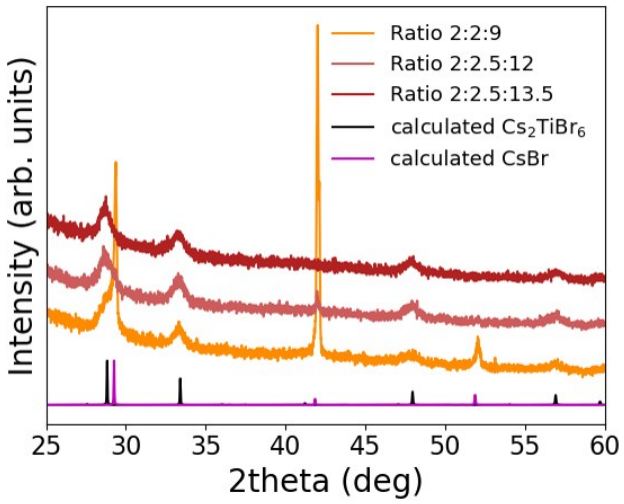

Figure S1. XRD patterns of Cs_2TiBr_6 nanocrystals synthesized using three different precursors ´ratio (2:2:9, 2:2.5:12, 2:2.5:13.5). When using a ratio of 2:2:9, three strong diffraction peaks coming from CsBr contamination are visible in the XRD pattern, while when increasing the amount of bromide precursor injected into the solution up to a ratio of 2:2.5:13.5, these peaks are not visible anymore.

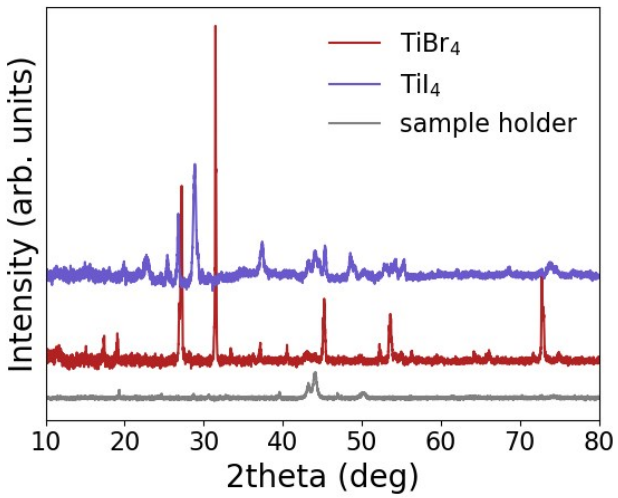

Figure S2. XRD patterns of $TiBr_4$ and TiI_4 powder taken using a special air-sensitive sample holder to avoid air contact.

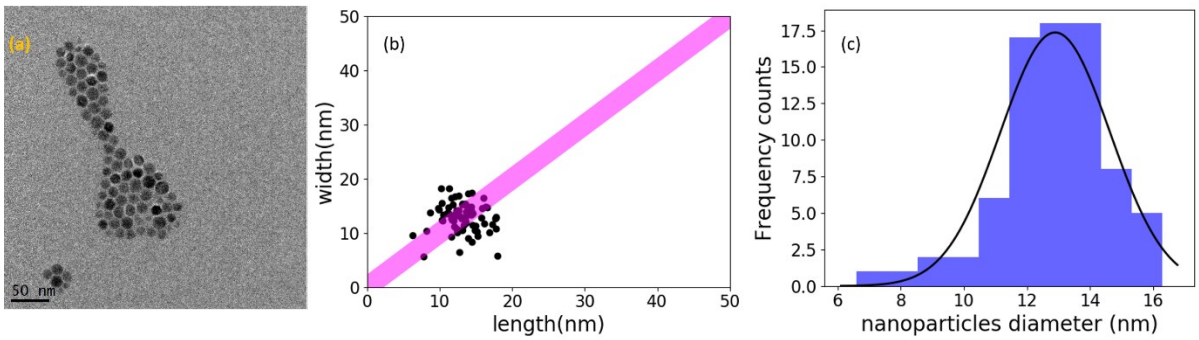

Figure S3. (a) TEM image from where the size distribution and symmetry analyses was carried out. (b) Histogram of the NCs diameters, calculated from the area of the NCs, indicating an average NC diameter of 12.9 nm, with a standard deviation of ± 1.7 nm. (c) Plot of the width vs the length of the nanoparticles, which indicates the nanoparticles are close to the symmetry.

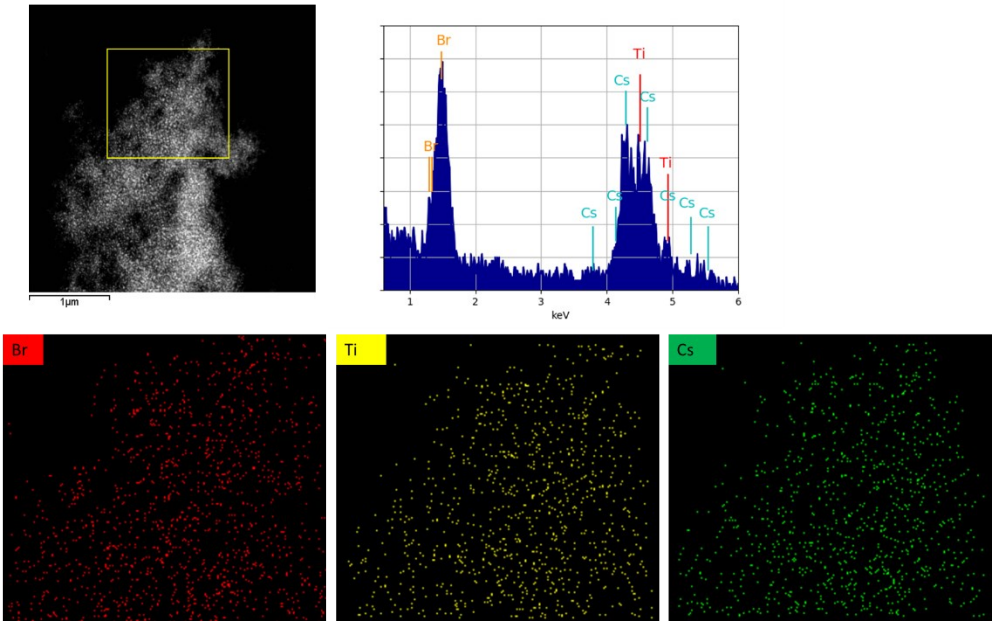

Figure S4. HAADF image and STEM-EDS analysis of Cs_2TiBr_6 NCs with the corresponding atomic maps.

ICP-OES results			
	Ti (mmols)	Cs (mmols)	Cs/Ti
Cs_2TiBr_6	0.027	0.057	2.1
Cs_2TiI_6	0.010	0.021	2.1
$Cs_2TiBr_3I_3$	0.030	0.060	2

Table S1. Elemental analysis using ICP-OES.

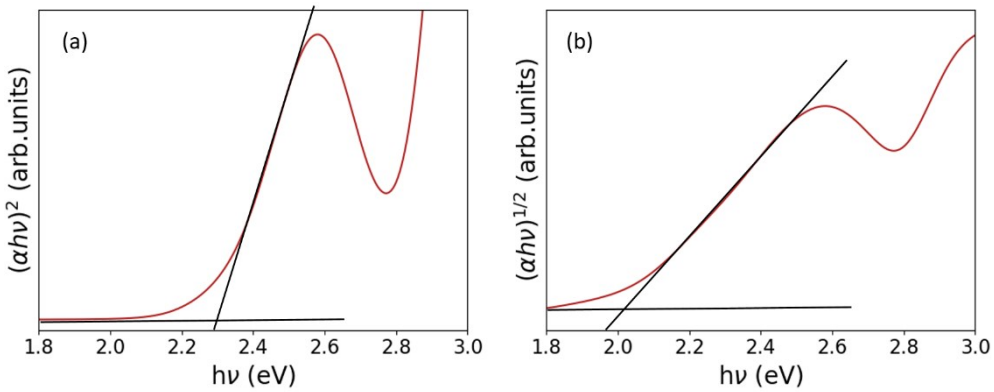

Figure S5. Tauc Plot of Cs_2TiBr_6, considering direct bandgap (a) and indirect bandgap (b).

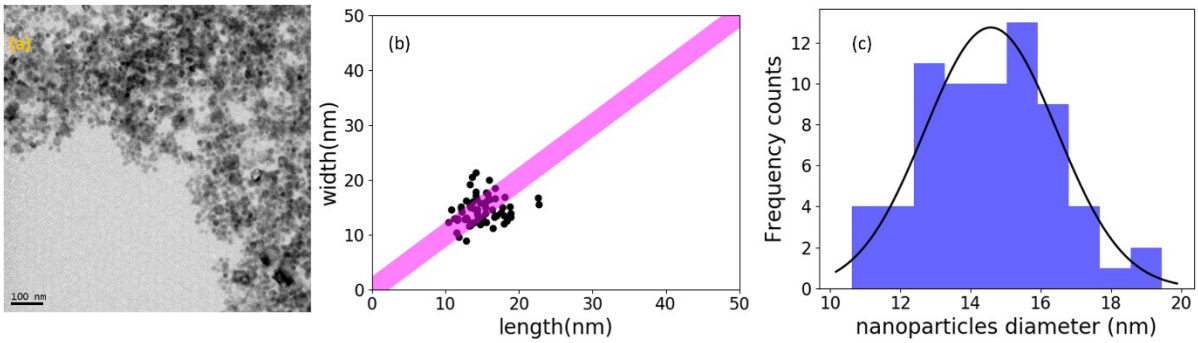

Figure S6. (a) TEM image of Cs_2TiBr_6 nanoparticles prepared using only oleic acid and quenching the reaction by diluting the solution with toluene. (b) Histogram of the NCs diameters, calculated from the area of the NCs, indicating an average NC diameter of 14.7 nm, with a standard deviation of around 1.9 nm. (c) Plot of the width vs the length of the nanoparticles, which indicates the nanoparticles are close to the symmetry.

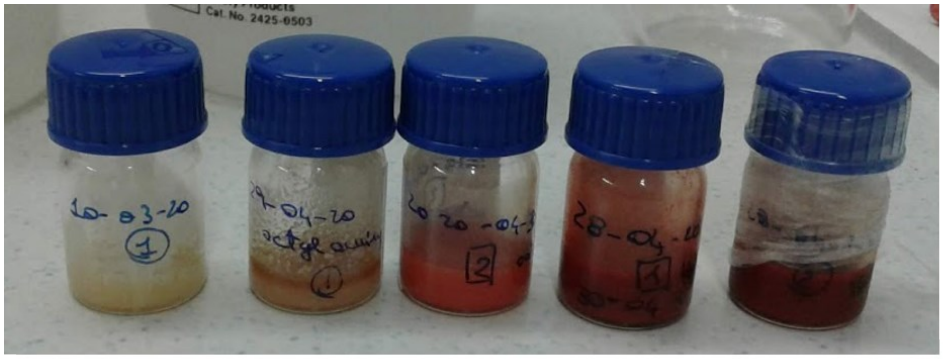

oleylamine | octylamine | octylamine at 90°C | octylamine at room T | oleic acid

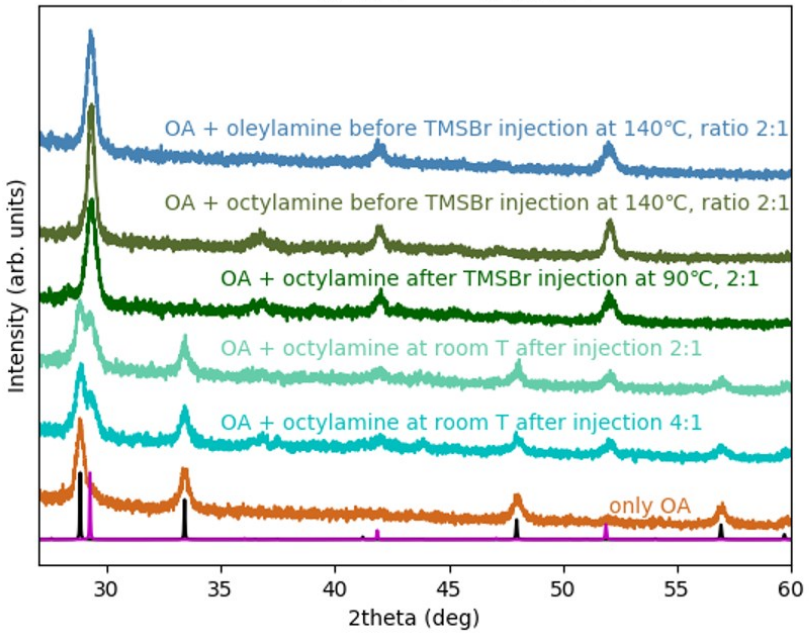

Figure S7. Comparison of solutions prepared adding oleylamine and octylamine in different amounts (indicated as ratio oleic acid/amine) and at different temperatures. The black pattern is the Cs_2TiBr_6 reference and the purple one the CsBr reference.

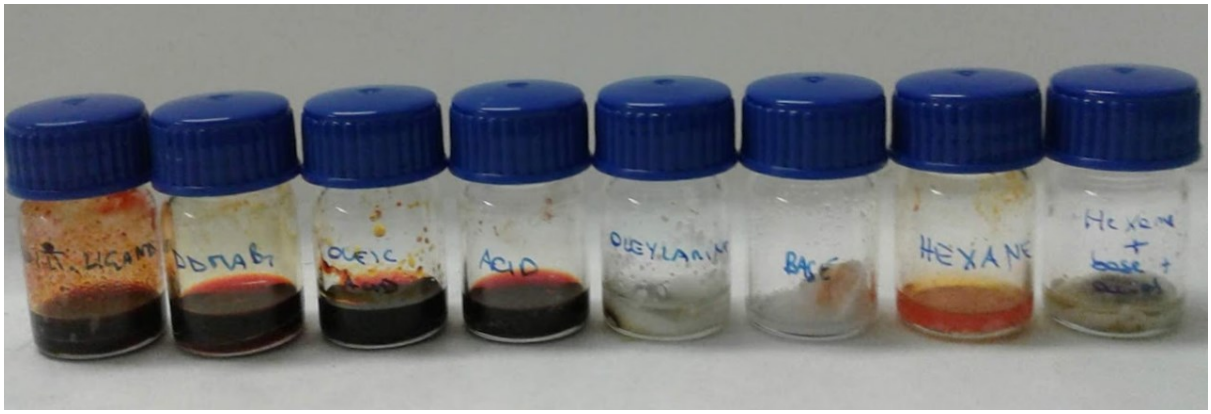

Figure S8. Comparison of the effect of adding different ligands into a solution of $TiBr_4$ dissolved in toluene. In order, 3-(N,N-dimethyloctadecylammonio)propanesulfonate, didodecyldimethylammonium bromide, oleic acid, propionic acid, oleylamine, butylamine, hexane and hexane with propionic acid and butylamine.

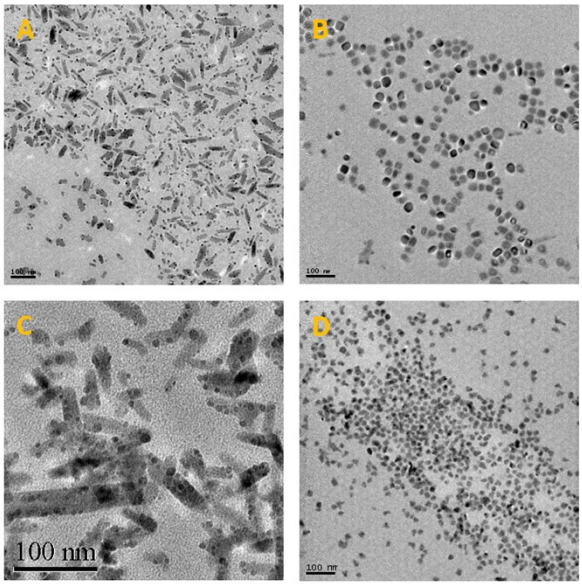

Figure S9. Effect of the different quenching method. TEM image of Cs_2TiBr_6 NCs prepared with oleic acid and the zwitterionic ligand using (a) the water bath and (b) the dilution in toluene to quench the reaction. TEM image of Cs_2TiBr_6 NCs prepared only with oleic acid and using (c) the water bath and (d) the dilution in toluene to quench the reaction.

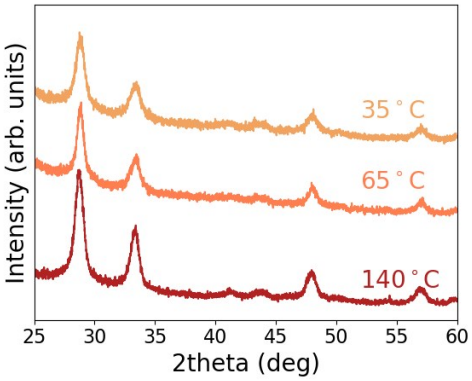

Figure S10. XRD patterns of Cs_2TiBr_6 produced at different temperatures.

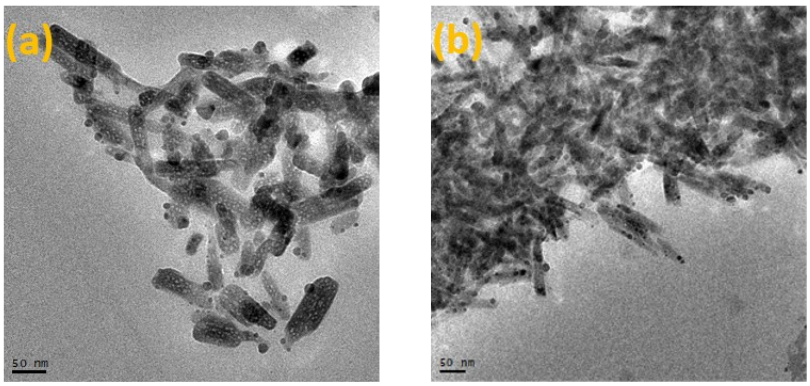

Figure S11. TEM images of NCs produced at 35°C (a) and 65°C (b).

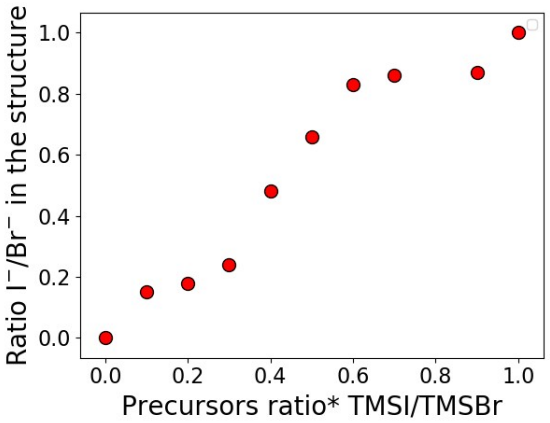

Figure S12. Ratio iodide/bromide in the structure of the perovskite vs precursors' ratio, which is the ratio of the precursors taking into account the optimal X moles for the two pure halide perovskites'syntheses.*

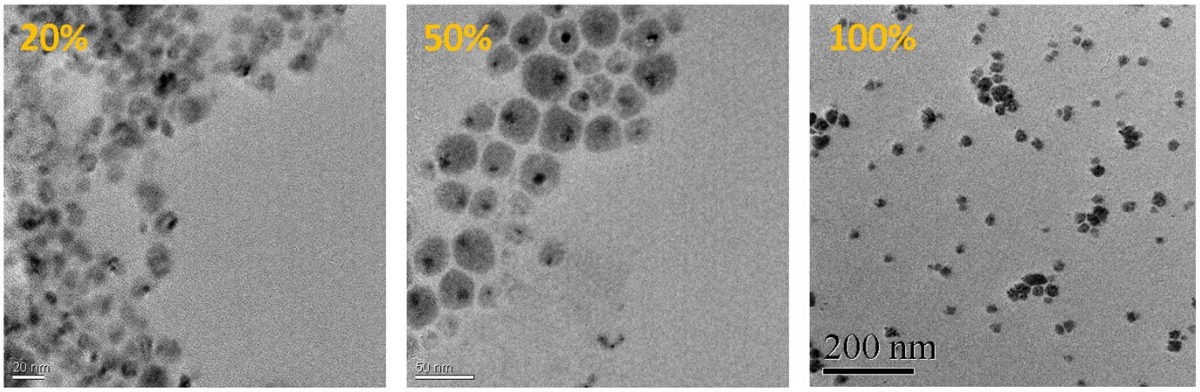

Figure S13. TEM images for two mixed halides and pure iodide $Cs_2TiBr_{6-x}I_x$ NCs.

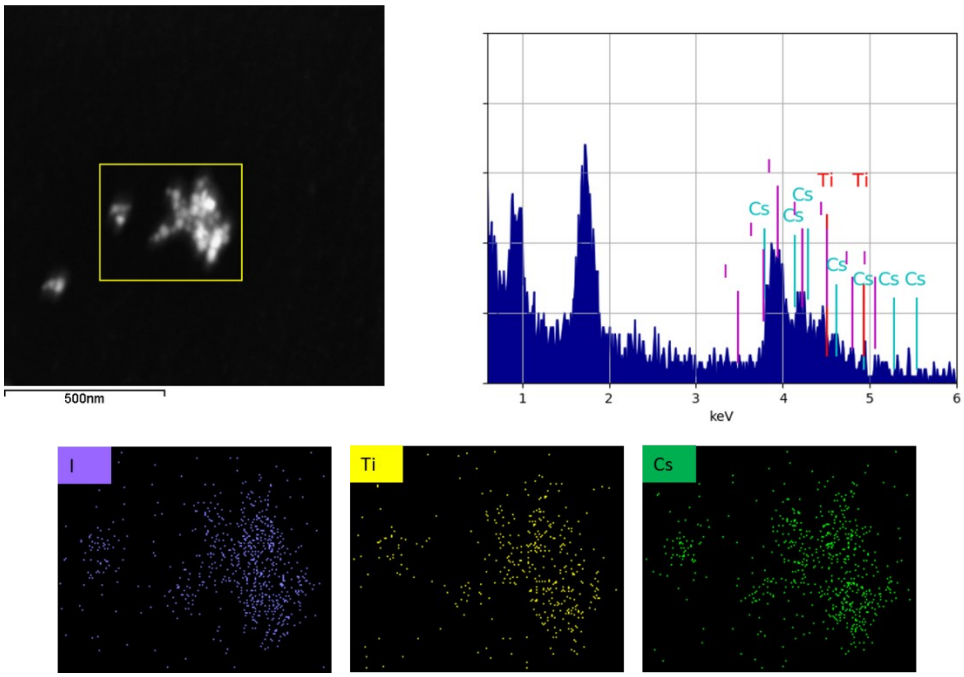

Figure S14. HAADF image and STEM-EDS analysis of Cs_2TiI_6 NCs with the corresponding atomic maps. In the spectrum, the peaks at 0.93 and 1.74 keV are due to copper of the TEM grid and silicon contamination coming from the Si(Li) detector, respectively.

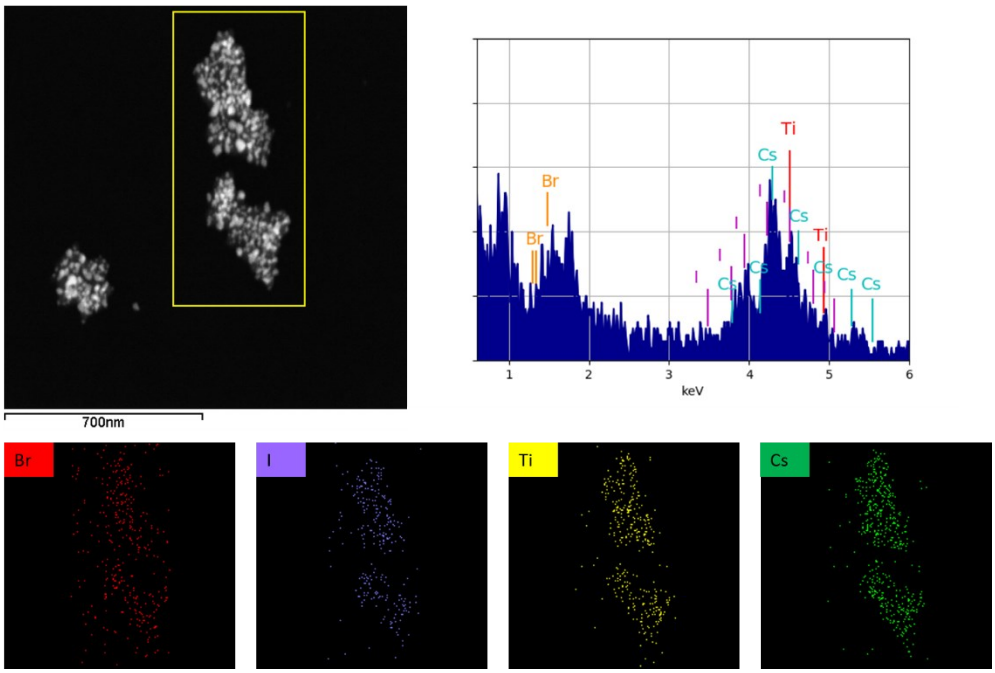

Figure S15. HAADF image and STEM-EDS analysis of the mixed-halide $Cs_2TiBr_xI_{6-x}$ sample prepared with the same amount of bromide and iodide precursors (50% sample) with the corresponding atomic maps.

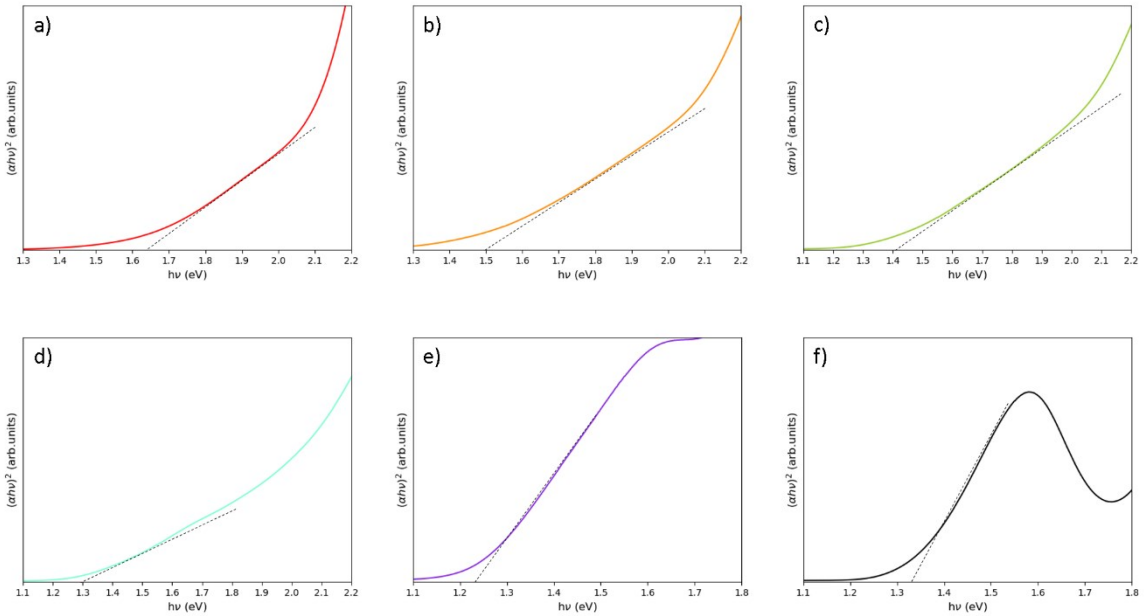

Figure S16. Tauc Plots of $Cs_2TiBr_{6-x}I_x$ NCs with a) 15%, b) 24%, c) 48%, d) 66%, e) 87% and f) 100% iodide in the structure.

Figure S17.Decomposition in air of a film prepared from a solution of Cs_2TiBr_6 drop-casted on glass in the glovebox after 5 and 10 minutes.

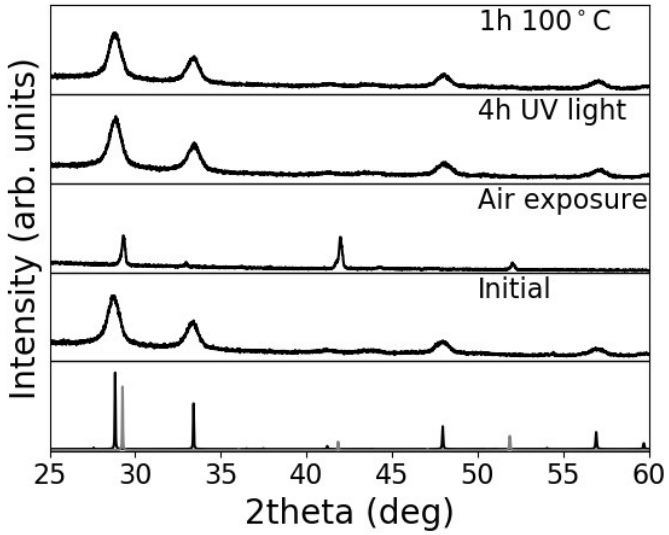

Figure S18. Stability of Cs_2TiBr_6 NCs films under different conditions together with the standard XRD patterns of Cs_2TiBr_6 (in black) and CsBr (in grey).

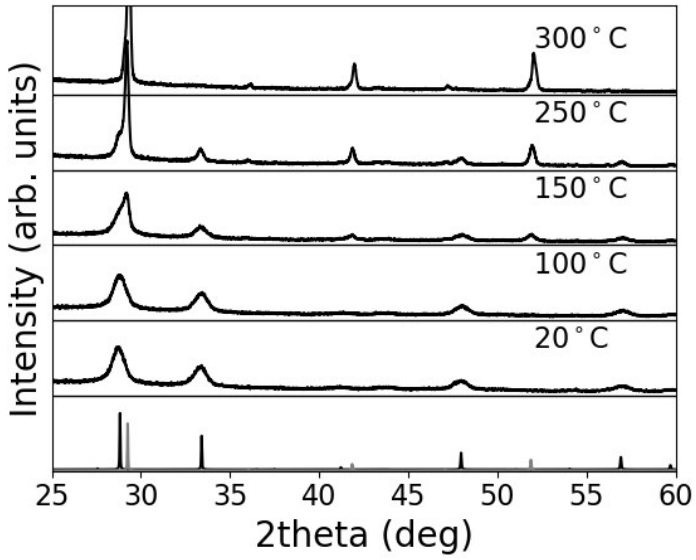

Figure S19. XRD of Cs_2TiBr_6 films after heating at different temperatures under Nitrogen atmosphere.